JOURNAL OF CATALYSIS 86, 266–279 (1984)

Surface Spectroscopic Characterization of the Interaction between Zinc Ions and γ-Alumina

BRIAN R. STROHMEIER AND DAVID M. HERCULES

Department of Chemistry, University of Pittsburgh, Pittsburgh, Pennsylvania 15260

Received June 23, 1983; revised October 14, 1983

Interaction of zinc ions with γ-alumina has been investigated using the surface spectroscopic techniques of X-ray photoelectron spectroscopy (ESCA or XPS) and low energy ion scattering spectroscopy (ISS). In addition, the "bulk" techniques of laser Raman spectroscopy (LRS) and X-ray diffraction (XRD) were employed. Surface characteristics of Zn/Al_2O_3 catalysts are affected by both metal loading and calcination temperature. The Zn/Al intensity ratio was examined as a function of zinc content and calcination temperature. Plots of both ESCA and ISS intensity ratios (Zn/Al) vs metal loading show changes in slope at high loadings, indicating a change in surface structure. ESCA, LRS, and XRD all show the ability to distinguish between ZnO and $ZnAl_2O_4$. Results indicate that at low zinc loadings (<20%), a strong interaction occurs between zinc and γ-alumina resulting in the formation of an "aluminate type" phase (i.e., a "surface spinel"). This interaction involves diffusion of zinc ions into the tetrahedral lattice sites of the support. At higher loadings, bulk-like ZnO segregates on top of the interaction species and the support. ESCA has also been used to study the effects of reduction and sulfiding on the catalysts.

INTRODUCTION

During the past decade much work has been published on alumina-supported transition metal catalysts. This growing interest has arisen because of the increasing number and variety of industrial applications for which supported catalysts are used. Major interest has centered on catalysts such as $Co/Mo/Al_2O_3$, Cu/Al_2O_3, Ni/Al_2O_3, and similar catalysts because of their importance for many industrial processes (*1*). Most studies have focused on interactions between the metal and support, since metal–support interactions are known to have a pronounced effect on the surface properties and reactivities of supported catalysts.

The present study involves investigation of the interaction between zinc ions and γ-alumina. In contrast to other supported catalysts, Zn/Al_2O_3 catalysts have not been extensively studied, although they have been studied briefly by X-ray photoelectron spectroscopy (ESCA or XPS) (*2*) and low energy ion scattering spectroscopy (ISS) (*3*). This lack of study is probably due to the lack of application of Zn/Al_2O_3 catalysts in industrial processes compared with other transition metal catalysts. However, Zn/Al_2O_3 catalysts have been shown to be active for the elimination of HCl from 1- and 2-chlorobutane and for the isomerization of 1-butene to isobutene (*2, 4, 5*).

Despite the limited application of Zn/Al_2O_3 catalysts, the interaction of zinc ions with γ-alumina is of considerable interest for several reasons. By determining what types of metal–support interactions occur in Zn/Al_2O_3 catalysts, a better understanding of metal–support interactions in similar catalytic systems (i.e., Ni/Al_2O_3, Co/Al_2O_3) can be gained. Also, $Cu/Zn/Al_2O_3$ catalysts are important industrial catalysts for the low pressure synthesis of methanol and the low temperature water–gas shift reaction (*6, 7*). The Zn/Al_2O_3 system represents a useful starting point for characterizing the more complex $Cu/Zn/Al_2O_3$ system. Also, it has been shown recently that addition of a small quantity of Zn^{2+} ions to γ-Al_2O_3 can drastically influence the surface properties of both Ni/Al_2O_3 (*8*) and Co/Al_2O_3 (*3, 9*)

0021-9517/84 $3.00

catalysts. By studying the interaction between zinc and γ-alumina, the influence of zinc addition on these catalytic systems may be better understood. The effect of zinc content on the dispersion and nature of surface species formed on Co/Al_2O_3 catalysts is currently being investigated (*10*).

The surface properties of two series of Zn/Al_2O_3 catalysts have been investigated in the present study. Surface characterization of these catalysts has been performed as a function of metal loading (1–26%) and calcination temperature (400 or 600°C). Emphasis is on how these two factors affect metal–support interactions. The surface spectroscopic techniques of ESCA and ISS, as well as the "bulk" techniques of laser Raman spectroscopy (LRS) and X-ray diffraction (XRD), have been employed to characterize the catalysts. In addition to spectroscopic investigations, reactivity of the catalysts to H_2 reduction and sulfiding with H_2S/H_2 and SO_2/air mixtures has been evaluated. The reactivity of the catalysts is of interest as a diagnostic tool to distinguish between different surface species by taking advantage of changes in ESCA spectra caused by differences in chemical reactivity.

EXPERIMENTAL

Catalyst preparation. Two series of Zn/Al_2O_3 catalysts were prepared by wet impregnation of γ-Al_2O_3 (Harshaw Chemical Co., Alumina #AL-1401P, BET surface area: 195 m^2/g) with an aqueous zinc nitrate solution. Excess water was evaporated at 90°C, with stirring. Samples were dried for 24 hr at 110°C, finely ground, and subsequently calcined in dry air for 5 hr at either 400 or 600°C. $Zn(NO_3)_2$ decomposed completely after calcination as indicated by the lack of a N 1s signal in the wide scan ESCA spectrum.

Standard materials. All reference compounds, with the exception of $ZnAl_2O_4$, were obtained from Alfa Products and were used without further purification. The composition of all standard compounds was confirmed by XRD. Experimental XRD patterns of all reference compounds matched the appropriate ASTM powder diffraction file, with no stray lines being present.

$ZnAl_2O_4$ was prepared by mixing stoichiometric amounts of ZnO and γ-Al_2O_3 with a small amount of deionized H_2O and mulling into a paste. The paste was dried for 8 hr at 110°C, finely ground, and subsequently calcined for 72 hr at 900°C. Formation of zinc aluminate was confirmed by XRD. The XRD pattern also showed several weak peaks which were assigned to ZnO. ZnO is readily soluble in aqueous ammonia, whereas $ZnAl_2O_4$ is only slightly soluble in ammonia (*11*). The $ZnAl_2O_4$ was, therefore, repeatedly washed with 1 *M* $(NH_4)_2CO_3$, rinsed with deionized H_2O, filtered, and dried at 110°C overnight. The XRD pattern of the resulting solid exactly matched the ASTM powder diffraction file for $ZnAl_2O_4$; ZnO peaks were absent.

ESCA spectra. ESCA spectra were obtained with an AEI ES200A electron spectrometer equipped with an AEI DS100 data system interfaced to an Apple II plus (48K) microcomputer. The spectrometer utilized nonmonochromatized Al$K\alpha$ radiation (1486.6 eV). The anode was operated at 12 kV and 22 mA. The instrument typically operates at pressures below 5×10^{-8} Torr. Samples were mounted in the form of a powder on a water-cooled aluminum probe using Scotch brand double-sided tape.

ESCA binding energies and intensity ratios are reported as the average of at least three separate determinations. Binding energies were measured with a precision of ±0.15 eV or better. For catalyst samples, the Al 2p line (74.5 eV) of the alumina support was used as an internal reference for determination of binding energies. The binding energy of the Al 2p line was determined by vacuum deposition of gold on γ-Al_2O_3, referencing to the Au $4f_{7/2}$ line (83.8 eV) (*3*). The average C 1s binding energy obtained on γ-Al_2O_3 and all catalyst samples was 285.1 eV. Therefore, binding energies for all standard compounds were refer-

enced to the C 1s line (285.1 eV). ESCA intensity ratios were determined using the total integrated areas of the Zn $2p_{3/2}$ and Al 2p lines. Integrated peak areas were calculated assuming that the background was linear over the peak width. Intensity ratios were reproducible to ±8% (r.s.d.) or better.

ISS spectra. ISS spectra were recorded using a 3M Model 525/610 ISS/SIMS spectrometer which employed a cylindrical mirror analyzer (CMA) to measure the energy of the backscattered ions. Monoenergetic $^4He^+$ ions were used with a primary-ion energy of 2.0 kV. The primary ion current density was ca. 2.0×10^{-7} A/cm^2. A typical base pressure of 5×10^{-9} Torr was achieved before the helium was admitted to the spectrometer. Spectra were obtained with a helium pressure in the sample chamber of 2.0×10^{-5} Torr. Samples (ca. 50 mg) were pressed into pellets (6 × 15 mm) under approximately 5000 psi and mounted on an aluminum probe with double-sided tape. Charge neutralization was accomplished by thermal electron emission from a resistively heated thoriated tungsten filament operated at 2 mA. The E/E_0 region from 0.3 to 1.0 was recorded with a scan time of approximately 3 min. ISS intensity ratios were determined using the Zn and Al peak heights. Peak heights were manually measured, assuming a linear background over the peak width. Plotted peak height intensities are the averages of at least three separate determinations.

Laser Raman spectra. Raman spectra were recorded with a Spex Ramalog spectrometer equipped with holographic gratings. The 514.5 nm line from a Spectra-Physics Model No. 165 argon-ion laser was used as the excitation source. Approximately 45 mW of power (measured at the sample) was employed. The spectral slit width was typically 4 cm^{-1}, and reported peaks are accurate to ±2 cm^{-1}. Samples were pressed into pellets with a small amount of KBr as a support. To avoid decomposition from the laser beam, samples were rotated off axis during analysis.

X-ray diffraction. X-Ray powder diffraction patterns were obtained at room temperature using a Diano Model 700 diffractometer employing Ni filtered Cu$K\alpha$ radiation (1.54056 Å). The X-ray tube was operated at 50 kV and 25 mA. Samples were packed into a plastic holder having a 18 × 18 × 2 mm opening. No binder or adhesive was used. Spectra were scanned at a rate of 0.4° min^{-1} (in 2θ). Spectra were compared with the ASTM powder diffraction files for compound identification.

Chemical analysis. Bulk Zn concentrations (wgt %) were determined by atomic absorption spectroscopy using a Perkin Elmer Model 2380 AA spectrophotometer. Catalyst samples were dissolved by digestion in concentrated nitric acid. For the sake of simplicity, all metal concentrations are reported as integral values. Actual concentrations are within ±0.2% (absolute) of the stated values.

Chemical reactions. All samples were pressed into pellets prior to gas-phase reactions. To confirm that the pelleting process did not induce chemical changes in the catalyst, the ESCA binding energies and Zn/Al intensity ratios for samples dusted onto double-sided tape were compared with the values obtained for samples pressed as pellets. No differences were observed; hence, it was assumed that the original powdered catalysts were identical with the pressed catalysts.

Samples were mounted on an air-cooled sealable probe with stainless-steel clips. The probe allows the transfer of samples from the reaction chamber to the ESCA spectrometer without exposure to air. The probe and reaction chamber have been described previously (*12*). The sample probe was inserted into the reaction chamber in the sealed position, while the chamber was heated to the desired temperature and allowed to equilibrate under gas flow (50 ml/min). Once the desired temperature was reached (ca. 30 min), the probe was opened and the reaction was allowed to proceed for a specified length of time. After the reaction

was completed, the probe was closed, allowed to cool, and then transferred to the spectrometer.

For reduction studies, pure H_2 (Air Products 99.999%) was employed for 5 hr at 500°C. Sulfiding reactions were accomplished with either 15% H_2S/H_2 (Air Products) or 1.5% SO_2/air (Matheson) for 1 hr at 350°C. All gases were used as received without further purification.

RESULTS

XRD Results

Lo Jacono and Schiavello have reported that when transition metal ions (Mn^{2+}, Co^{2+}, Ni^{2+}, Cu^{2+}) are supported on alumina, formation of a "surface spinel" or bulk-like metal-oxide occurs, often concurrently (*13*). Hence, when Zn^{2+} ions are dispersed on γ-Al_2O_3, two likely reactions are formation of an "aluminate-type" phase (i.e., a "surface spinel") or formation of bulk-like ZnO.

XRD is used routinely to examine the build-up of bulk oxides at high metal loadings; however, identification of surface spinel phases by XRD has been difficult due to the lack of long-range order and because γ-Al_2O_3 itself has a defect spinel structure. Consequently, the lattice parameters of alumina are virtually identical to those of spinels (*13, 14*). Some of the major XRD lines for γ-Al_2O_3, $ZnAl_2O_4$, and ZnO are summarized in Table 1 (ASTM File Nos. 10-425, 5-0664, 5-0669); the peaks at $d \cong 2.4$ and 2.8 Å (ca. 37 and 32°, 2θ) closely coincide for all three compounds. Lo Jacono and Schiavello (*13*) have shown that the relative intensities of certain diffraction lines show characteristic behavior which indicates formation of spinel-like structures. They found that the intensities of the lines at approximately $d = 2.4$ and 2.8 Å (strong lines for spinels) increase for aluminas containing transition metal ions. We have observed this effect for Zn/Al_2O_3 catalysts.

The experimental XRD patterns obtained for $ZnAl_2O_4$, ZnO, γ-Al_2O_3, and several Zn/Al_2O_3 catalysts are shown in Fig. 1. The γ-Al_2O_3 support gave broad, diffuse, diffraction lines (Fig. 1C), indicating poor crystallinity. For catalysts having zinc loadings below 10%, XRD patterns were virtually identical to the support pattern. At these low loadings, zinc is probably too highly dispersed to cause any noticeable change in the alumina structure. At zinc loadings greater than 10%, the intensities of the lines at approximately 32 and 37° begin to increase, relative to the main alumina

TABLE 1

Major XRD Lines for Reference Compounds (Cu$K\alpha$ Radiation)

γ-Al_2O_3			$ZnAl_2O_4$			ZnO		
d(Å)	2θ	I/I_0	d(Å)	2θ	I/I_0	d(Å)	2θ	I/I_0
2.80	31.9	20	2.86	31.2	84	2.82	31.7	71
2.39	37.6	80	2.44	36.8	100	2.60	34.4	56
2.28	39.5	50				2.48	36.2	100
1.97	46.0	100				1.91	47.5	29

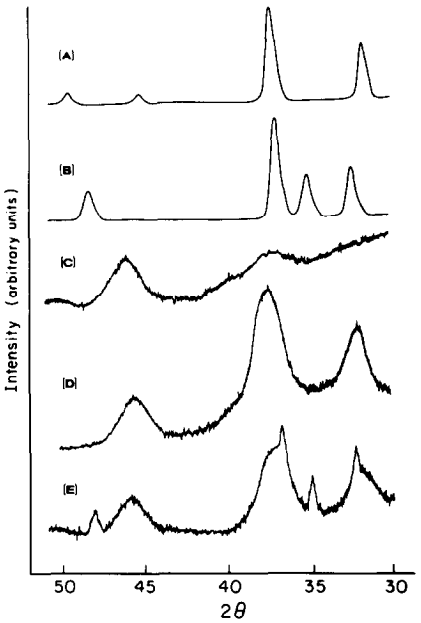

FIG. 1. X-Ray powder diffraction patterns of reference compounds and Zn/Al_2O_3 catalysts: (A) $ZnAl_2O_4$; (B) ZnO; (C) γ-Al_2O_3; (D) 18% Zn/Al_2O_3 (600°C); (E) 22% Zn/Al_2O_3 (400°C).

line ($2\theta = 46°$). With increased zinc loading, the lines at 32 and 37° became narrower and more intense, consistent with formation of a spinel-like phase. An example of this behavior is seen in Fig. 1D, which shows the XRD pattern of an 18% Zn/Al_2O_3 (600°C) catalyst. One can easily see the significant increase in intensity of the lines at ca. 32 and 37° compared to the pattern for γ-Al_2O_3. This increase in intensity cannot be attributed to ZnO formation, as the other major lines in the ZnO pattern (34.4 and 47.5°) were absent.

Neither γ-Al_2O_3 nor $ZnAl_2O_4$ has lines at 34.4 or 47.5°, therefore, these lines are convenient for determining segregation of bulk-like ZnO. No lines were seen at 34.4 or 47.5° for catalysts containing less than 20% Zn. At 20% loading, however, weak peaks became evident at approximately 34 and 47°, becoming more intense with increasing Zn content (>20%). In addition, shoulders appeared on the spinel lines at ca. 32 and 37° (see Fig. 1E), because the most intense peaks of the surface spinel and ZnO overlap. Comparison of Fig. 1E (22% Zn/Al_2O_3, 400°C) with 1B (ZnO), confirms build-up of a ZnO phase at high zinc loadings. XRD patterns of catalysts having identical zinc loadings but calcined at different temperatures, showed little difference.

The colors of the catalysts were consistent with formation of ZnO at high Zn loadings. Following calcination, all catalysts were white with the exception of those containing greater than 20% Zn (both 400 and 600°C). These catalysts were slightly yellow; $ZnAl_2O_4$ and ZnO are both normally white, but ZnO is known to become yellow on heating (*15*). It was also observed that upon removal from the muffle furnace after calcination, catalysts containing greater than 20% Zn thermoluminesced bright yellow for several minutes while cooling. ZnO thermoluminesces whereas $ZnAl_2O_4$ does not; $ZnAl_2O_4$ shows no color change during or after heating.

ESCA Results

The ESCA binding energies of relevant zinc reference compounds and of γ-Al_2O_3 are summarized in Table 2. $ZnAl_2O_4$ and ZnO are useful reference compounds to model phases which may exist on oxidic Zn/Al_2O_3 catalysts, whereas Zn°, ZnS, and $ZnSO_4$ are useful models for reduction and sulfiding studies. However, exact matching of ESCA binding energies is not a sufficient criterion to confirm species on a catalyst surface. Vinek *et al.* have reported ESCA binding energies for the Zn $2p_{3/2}$ and Zn 3p lines of both ZnO and $ZnAl_2O_4$ (*2*). They found chemical shifts (relative to the C 1s line) between ZnO and $ZnAl_2O_4$ of 0.6 eV for the Zn $2p_{3/2}$ line, and 0.8 eV for the Zn 3p line. The data of Table 2 show shifts of

TABLE 2

ESCA Binding Energies[a] (eV) for Zinc Reference Compounds

Sample	Zn $2p_{3/2}$	Zn LMM Auger[b]	Zn Auger parameter[c]	Zn $2p_{1/2}$	Zn 3p	Zn 3s	O 1s	Al 2p	Al 2s	S 2p	S 2s	C 1s
γ-Al_2O_3[d]	—	—	—	—	—	—	531.3	74.5	119.3	—	—	285.1
ZnO[e]	1021.5	988.6	532.5	1044.6	88.6	139.5	530.2	—	—	—	—	285.1
$ZnAl_2O_4$[d]	1022.0	987.5	522.9	1045.1	89.4	140.3	531.3	74.5	119.3	—	—	285.1
Zn[e]	1021.3	992.1	526.8	1044.4	89.0	140.1	—	—	—	—	—	285.1
$ZnSO_4$[e]	1021.3	985.9	520.6	1046.2	90.6	141.5	533.0	—	—	170.1	233.9	285.1
ZnS[e]	1022.0	989.3	524.7	1045.1	89.2	140.2	—	—	—	162.3	226.3	285.1

[a] Binding energies (B.E.s) were measured with a precision of ±0.15 eV or better.
[b] Auger values in kinetic energy.
[c] K. E. (Zn LMM Auger) − K.E. (Zn $2p_{3/2}$); see Ref. *18*.
[d] B.E.s referenced to Al 2p = 74.5 eV.
[e] B.E.s referenced to C 1s = 285.1 eV.

0.5 eV ($2p_{3/2}$) and 0.8 eV (3p), in good agreement with the earlier results. The Zn $2p_{3/2}$ and Zn $L_3M_{4,5}M_{4,5}$ Auger lines were chosen to characterize Zn/Al_2O_3 catalysts because they are the most intense zinc lines in the ESCA spectrum. As can be seen from Table 2, the Zn LMM Auger line shows a chemical shift of 1.1 eV between ZnO and $ZnAl_2O_4$. Even though the chemical shifts for the $2p_{3/2}$ and Auger lines are relatively small, they allow one to distinguish between ZnO and $ZnAl_2O_4$ on the catalyst surface.

The Zn $2p_{3/2}$ and LMM Auger lines for $ZnAl_2O_4$, ZnO, and Zn° are shown in Fig. 2. Figure 2 shows small chemical shifts and similar band shapes for the Zn $2p_{3/2}$ lines of $ZnAl_2O_4$, ZnO, and Zn°. A chemical shift of 0.2 eV was found between the Zn $2p_{3/2}$ lines of ZnO and Zn metal. Previous investigators have reported chemical shifts ranging from 0 to 0.3 eV (*16, 17*). Such small chemical shifts would make distinction between ZnO and Zn metal difficult. However, the LMM Auger lines of ZnO and Zn metal are separated by 3.5 eV and have very different band shapes, allowing easy distinction between ZnO and Zn metal.

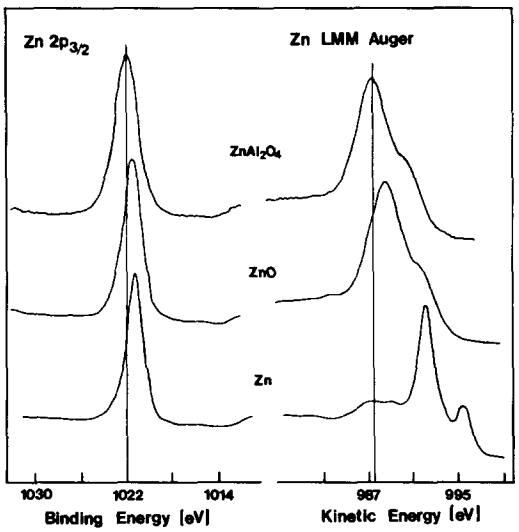

FIG. 2. ESCA spectra of the Zn $2p_{3/2}$ and Zn LMM Auger lines for zinc reference compounds: $ZnAl_2O_4$, ZnO, Zn°.

The Auger band shapes for ZnO and $ZnAl_2O_4$ are virtually identical (although shifted by 1.1 eV). However, as noted, the Auger line for Zn metal has a different band shape. All of the Auger bands consist of two peaks, although they are poorly resolved for ZnO and $ZnAl_2O_4$. The origin of the doublets is believed to arise from 1-s coupling (*17*). The line width of the Auger peak is much narrower for Zn metal than for ZnO or $ZnAl_2O_4$, presumably due to different transition probabilities and lifetimes in the final states (*17*). Because the Auger lines show larger chemical shifts, they are more sensitive to the chemical environment. Also, the Auger parameter (kinetic energy of the Auger line-kinetic energy of the photoelectron line) is useful for identifying chemical states (*18*). Hence, more attention should be paid to Auger lines in ESCA studies of catalysts. Most workers have focused only on photoelectron lines, and it is clear that Auger lines are useful for catalyst studies as well. The Auger parameters for the reference compounds are included in Table 2.

The ESCA binding energies of the catalysts studied are tabulated in Table 3. As can be seen, for Zn loadings from 1 to 18% (for both 400 and 600°C calcination) the binding energies for both the Zn $2p_{3/2}$ and LMM lines (Auger values in kinetic energy) are virtually identical with the values obtained for $ZnAl_2O_4$. However, at higher zinc contents (≥20 wt%), both lines begin to shift toward lower binding energies, indicating a change in surface composition. At a zinc content of 26%, the binding energies of both the Zn $2p_{3/2}$ and Zn Auger lines are virtually identical with those of ZnO, consistent with formation of ZnO at high Zn loading as indicated by XRD.

The Zn $2p_{3/2}$/Al 2p ESCA intensity ratios plotted as a function of bulk Zn content are shown in Fig. 3 for calcination at 400 and 600°C. At all concentrations, the Zn/Al intensity ratios are lower for catalysts calcined at 600°C than for those calcined at 400°C. The intensity ratios are linear with

TABLE 3

ESCA Binding Energies[a] (eV) of Zn/Al_2O_3 Catalysts after Calcination at 400 and 600°C[b]

Zn/Al_2O_3 catalyst (%)	Calcination temperature			
	400°C		600°C	
	Zn $2p_{3/2}$	Zn LMM Auger[c]	Zn $2p_{3/2}$	Zn LMM Auger
1	1022.0	987.2	1022.0	987.5
2	1022.0	987.5	1022.0	987.6
3	1022.0	987.2	1022.0	987.4
5	1021.9	987.3	1022.0	987.5
8	1022.0	987.3	1022.0	987.5
10	1022.0	987.5	1022.0	987.5
14	1022.1	987.4	1022.0	987.5
18	1022.0	987.5	1022.0	987.5
20	1021.8	987.6	1021.7	987.6
22	1021.7	987.8	1021.5	988.1
26	1021.5	988.2	1021.5	988.6

[a] All B.E.s referenced to Al 2p = 74.5 eV.
[b] All catalysts showed the following average binding energies (eV): Al 2s, 119.3; O 1s, 531.2; C 1s, 285.1.
[c] Auger values in kinetic energy.
[d] B.E.s were measured with a precision of ±0.15 eV or better.

zinc content for loadings below 20%, but there is an abrupt change in slope at ~20%. The change in slope indicates that an alteration in surface composition occurs at about 20% Zn. It is interesting to note that the change in slope occurs at the same concentration at which the ESCA binding energies began to shift, consistent with a change in surface composition.

ISS Results

Typical ISS spectra of Zn/Al_2O_3 catalysts are shown in Fig. 4. The Zn/Al ISS intensity ratio is influenced by both zinc content and calcination temperature. The Zn/Al ISS intensity ratio as a function of zinc content and calcination temperature is shown in Fig. 5. The results are consistent with the ESCA data. The Zn/Al intensity ratio is linear for zinc contents up to approximately 20% Zn (at both 400 and 600°C). Above 20% Zn, there is an increase in the slopes of the curves, indicating a change in surface composition. Figure 5 also shows that the Zn/Al intensity ratios for catalysts calcined at 400°C are larger than for catalysts calcined at 600°C.

ISS could detect the presence of zinc over the entire concentration range studied (1–26% Zn) for catalysts calcined at 400°C. However, for catalysts calcined at 600°C, ISS could not detect zinc at loadings below 3% Zn. After prolonged sputtering (ca. 15–20 min) weak Zn peaks became evident for

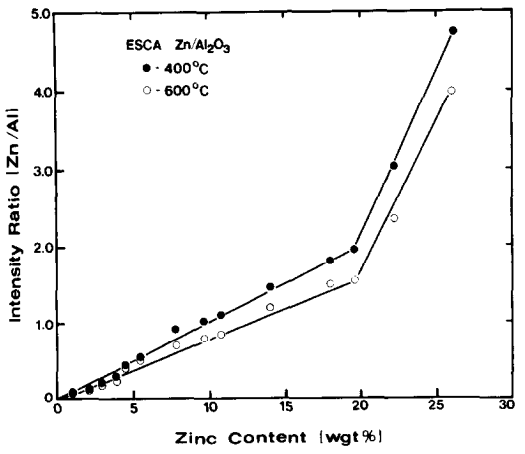

FIG. 3. ESCA Zn $2p_{3/2}$/Al 2p intensity ratio vs bulk zinc content at different calcination temperatures: (●) 400°C; (○) 600°C.

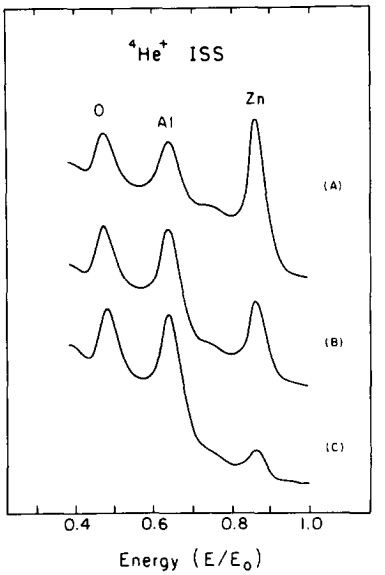

FIG. 4. ISS spectra of Zn/Al_2O_3 catalysts calcined at 400°C: (A) 22% Zn; (B) 8% Zn; (C) 3% Zn.

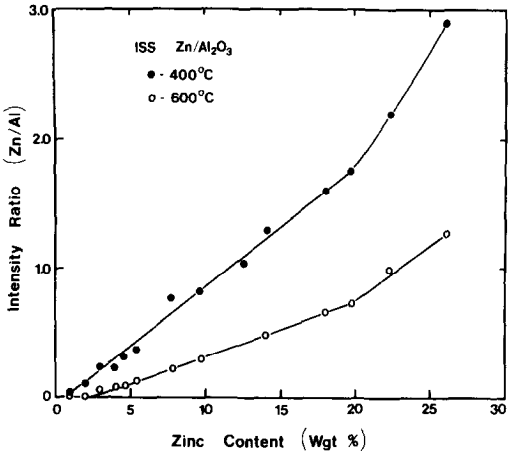

FIG. 5. ISS Zn/Al peak height intensity ratio vs bulk zinc content at different calcination temperatures: (●) 400°C; (○) 600°C.

catalysts containing less than 3% Zn (600°C). Since ISS is sensitive to the uppermost atomic layer, these results imply that all of the zinc ions are below the first atomic layer, shielded from the ion beam, for catalysts calcined at 600°C and containing less than 3% Zn, therefore, the zinc is undetected until the upper surface layer is sputtered away. Shelef *et al.*, in an ISS study of spinels, reported similar results for bulk $ZnAl_2O_4$; only after several scans did a Zn peak become apparent (*19*).

Raman Results

Although LRS is generally considered to be a bulk technique, a recent study comparing ESCA, ISS, and LRS has shown that LRS can be sensitive to surface changes occurring within sampling depths characteristic of ESCA and ISS (*20*). To facilitate interpretation of the Raman spectra, LRS of several reference compounds were recorded, namely, ZnO, $ZnAl_2O_4$, and the γ-Al_2O_3 support. Spectra of the reference compounds are shown in Fig. 6 and the characteristic Raman bands are summarized in Table 4.

Figure 6A shows the Raman spectrum of bulk ZnO. The spectrum consists of a major band at 438 cm^{-1} (Zn–O stretch) and several weaker bands. The Raman frequencies

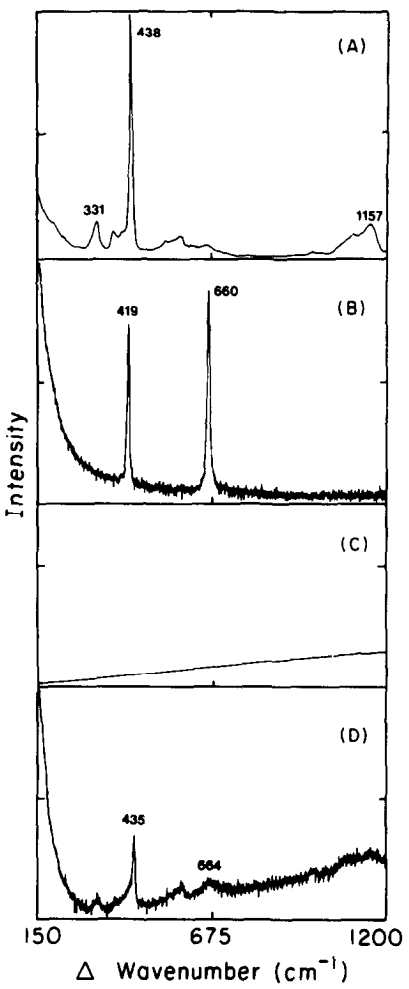

FIG. 6. Laser Raman spectra of reference compounds and Zn/Al_2O_3 catalysts: (A) ZnO; (B) $ZnAl_2O_4$; (C) γ-Al_2O_3; (D) 26% Zn/Al_2O_3 (600°C).

TABLE 4

Raman Bands of Reference Compounds[a]

Compound	Δ Wavenumber (cm^{-1})[b]
ZnO	1157(m), 1105(w), 1005(vw), 982(vw) 659(w), 580(w), 540(w), 438(vs), 412(vw), 384(w), 331(m), 202(vw)
$ZnAl_2O_4$	660(s), 419(s)
γ-Al_2O_3	— — — —

[a] Intensities in parentheses: vs = very strong, s = strong, m = medium, w = weak, vw = very weak.
[b] All wavenumbers measured to ±2 cm^{-1}.

obtained for ZnO are in good agreement with values reported previously (*21*). The Raman spectrum of bulk $ZnAl_2O_4$ (Fig. 6B) consists of two bands at 660 and 419 cm^{-1}. Figure 6C shows the spectrum of the γ-Al_2O_3 support; as previously reported, no discrete scattering is apparent in the region of interest (*20*).

The Raman spectra obtained for catalysts containing 15% Zn or less, calcined at either 400 or 600°C, were identical with the spectrum obtained for γ-Al_2O_3, showing no evidence of any zinc species. Because γ-Al_2O_3 has a strong scattering ("fluorescence") background (attributed to the presence of hydroxyl groups or trace contamination on the surface) detection of Raman bands (*22*) is limited. While the presence of a $ZnAl_2O_4$-like phase could not be confirmed at these low loadings, the lack of peaks characteristic of ZnO is significant and consistent with the XRD and ESCA results. However, at 18% Zn, two weak, broad bands characteristic of a $ZnAl_2O_4$-like phase were observed in the Raman spectra.

For catalysts containing 20% Zn or more, additional LRS peaks were seen which indicated the presence of ZnO. Figure 6D shows the Raman spectrum of a Zn/Al_2O_3 catalyst containing 26% Zn (600°C). The spectrum shows a main band at 435 cm^{-1} and several weaker bands at 664, 581, and 330 cm^{-1}. Within experimental error, these values correspond to the major bands of bulk ZnO. However, the broadness and intensity of the band at 664 cm^{-1} and broadening on the low frequency side of the 435 cm^{-1} band (see Fig. 6D) indicate that an ill-defined $ZnAl_2O_4$ phase is also present.

REDUCTION STUDIES

Reduction characteristics of supported metal oxides are often different from those of bulk metal oxides because of metal-support interactions and changes in dispersion. It is well known that ZnO is not easily reduced, the reaction being thermodynamically unfavorable at 200°C (*7*):

$$ZnO + H_2 \rightarrow Zn + H_2O$$
$$\Delta G(200°C) = +19.2 \text{ kcal/mole.}$$

In this study, more drastic conditions were employed in an attempt to reduce the catalysts. At temperatures in excess of 700°C, ZnO readily sublimes (*23*); therefore, a temperature of 500°C (for 5 hr) was chosen for reduction. The conditions employed were previously found to be sufficient to reduce nickel, cobalt, and copper supported on alumina (*24–26*).

The effects of reduction on Zn/Al_2O_3 catalysts were monitored by ESCA. As discussed earlier, the Zn LMM Auger lines allow one to distinguish among ZnO, $ZnAl_2O_4$, and Zn metal (see Table 2). The results obtained in this study support the reported difficulty of reducing ZnO. Neither ZnO nor $ZnAl_2O_4$ was found to reduce under the conditions employed. Similar results were obtained for the catalysts. The ESCA binding energies and peak shapes of the Zn $2p_{3/2}$ line and the Zn LMM Auger line obtained for H_2 treated ZnO, $ZnAl_2O_4$, and catalyst samples (regardless of zinc loading or calcination temperature) were identical with the values obtained before treatment. XRD patterns of the H_2 treated samples also indicated no noticeable change in composition.

SULFIDING STUDIES

ZnO, both bulk and supported, has been widely used for removing impurities such as H_2S, mercaptans, and disulfides from gas streams (*1, 23*). In fact, one of the principal roles of zinc in $Cu/Zn/Al_2O_3$ catalysts is to protect the copper from poisoning by preferentially reacting with trace sulfur compounds (*6*). Hence, the reactivity of Zn/Al_2O_3 catalysts with sulfur compounds is of interest.

Two sulfiding mixtures were chosen for investigation, 15% H_2S/H_2 and 1.5% SO_2/air. H_2S and SO_2 were chosen as reactants because both are major industrial pollutants, usually removed from stack gases by sorption or by reaction with bulk or sup-

ported metal oxides (*1, 23, 27*). In this study, a reaction temperature of 350°C (1 hr) was chosen, as most industrial desulfurization processes operate in the range of 250–400°C (*1, 23, 27*).

To evaluate and compare the reactivities of the catalysts, the sulfiding properties of bulk ZnO and $ZnAl_2O_4$ were determined. While the binding energies of the Zn $2p_{3/2}$ lines are similar (see Table 2) for ZnO, $ZnAl_2O_4$, ZnS, and $ZnSO_4$, the Zn LMM Auger lines are sufficiently different in both energy and peak shape to distinguish among the compounds. The S 2p and S 2s binding energies also allow one to distinguish easily between ZnS and $ZnSO_4$. ESCA can, therefore, be used to determine surface species present after reaction by monitoring changes in the Zn Auger parameter and observing the absence or presence of the sulfur lines.

Table 5 lists the Zn Auger parameters, the S 2p and S 2s binding energies, and the S 2p/Zn $2p_{3/2}$ intensity ratios for ZnO and $ZnAl_2O_4$ after treatment (1 hr at 350°C) with 15% H_2S/H_2 and 1.5% SO_2/air. Included for comparison are the values obtained for bulk ZnS and $ZnSO_4$. The ESCA spectra of the Zn LMM Auger lines of ZnO and $ZnAl_2O_4$ are shown in Fig. 7. The ESCA spectrum of bulk ZnO, after treatment with 15% H_2S/H_2, showed very intense sulfur peaks and the absence of an O 1s peak. As seen in Table 5, the Zn Auger parameter, and the S 2p and S 2s binding energies were all within experimental error of the values obtained for bulk ZnS. Figure 7 clearly shows the similar Zn Auger spectra obtained for H_2S treated ZnO (Fig. 7B) and bulk ZnS (Fig. 7A). In addition, the S/Zn intensity ratio for treated ZnO was within experimental error of that the ZnS. This indicates that at least within the sampling depth of ESCA, ZnO was converted to ZnS. XRD patterns of the treated ZnO indicated the presence of ZnO; however, additional very weak peaks corresponding to ZnS were also seen by XRD.

TABLE 5

ESCA Results[a] for Sulfided Reference Compounds

Sample/treatment[b]	Zn Auger parameter	S 2p	S 2s	S 2p/Zn $2p_{3/2}$[c]
$ZnO/H_2S/H_2$	524.6	162.5	226.5	0.71
$ZnAl_2O_4/H_2S/H_2$	522.9	161.9	226.4	0.20
ZnO/SO_2/air	520.4	170.3	234.1	0.76
$ZnAl_2O_4/SO_2$/air	522.9	169.3	233.2	0.23
ZnS	524.7	162.3	226.3	0.78
$ZnSO_4$	520.6	170.1	233.9	0.84

[a] Binding energies in eV.
[b] Treatment for 1 hr at 350°C.
[c] All intensity ratios were measured with a precision of ±10% (r.s.d.) or better.

In contrast, the ESCA spectrum of H_2S treated $ZnAl_2O_4$ shows only weak sulfur peaks, indicating that little sulfiding occurred. In addition, the Zn Auger parameter for treated $ZnAl_2O_4$ was identical to that before treatment (see Tables 2 and 5), consistent with little reaction. Figure 7C shows that the Zn Auger spectrum of treated $ZnAl_2O_4$ is identical with that obtained for bulk $ZnAl_2O_4$ (see Fig. 2). Also, XRD patterns of the treated sample showed the presence of only $ZnAl_2O_4$. Similarly, $CoAl_2O_4$ is difficult to sulfide (*28*) but $CuAl_2O_4$ sulfides readily to yield Cu_2S (*26*).

The reactivity of ZnO and $ZnAl_2O_4$ to 1.5% SO_2/air was similar to the reactivity toward 15% H_2S/H_2. ZnO was found to react readily with SO_2. After treatment, the Zn Auger parameter, S 2p and S 2s binding energies, and the S/Zn intensity ratio were all within experimental error of the values obtained for $ZnSO_4$ (see Table 5). Figure 7 shows that the Zn Auger spectra for treated (1.5% SO_2/Air) ZnO (Fig. 7E) and $ZnSO_4$ (Fig. 7D) are identical. XRD patterns of SO_2 treated ZnO, however, showed no evidence of any sulfur compound, only the presence of ZnO. The formation of metal sulfates by the reaction of SO_2 with metal oxides has been reported previously by Vogel *et al.* (*27*).

The ESCA spectrum of SO_2 treated $ZnAl_2O_4$ as in the case for H_2S treatment, showed only weak sulfur peaks. The Zn Auger parameter for SO_2 treated $ZnAl_2O_4$ was identical with that obtained before

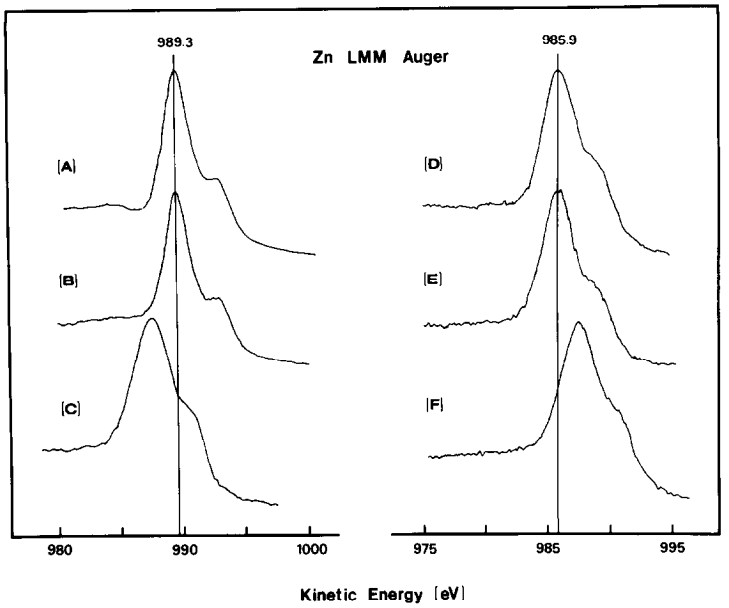

FIG. 7. ESCA spectra of the Zn LMM Auger line of sulfided ZnO, sulfided $ZnAl_2O_4$, and reference compounds: (A) ZnS; (B) 15% H_2S/H_2 treated ZnO; (C) 15% H_2S/H_2 treated $ZnAl_2O_4$; (D) $ZnSO_4$; (E) 1.5% SO_2/air treated ZnO; (F) 1.5% SO_2/air treated $ZnAl_2O_4$.

treatment, Figure 7F shows that the Zn Auger spectrum for SO_2 treated $ZnAl_2O_4$ is identical with that obtained for bulk $ZnAl_2O_4$ (see Fig. 2). XRD also indicated that there was no noticeable change in composition. Hence, the results indicate that essentially no sulfiding had occurred. The difference in reactivity toward H_2S and SO_2 between ZnO and $ZnAl_2O_4$ is useful for characterizing surface species on Zn/Al_2O_3 catalysts.

The reactivity of Zn/Al_2O_3 catalysts containing less than 20% Zn was similar to the reactivity of $ZnAl_2O_4$. The Zn Auger parameter for treated catalysts (either 15% H_2S/H_2 or 1.5% SO_2/air) was identical with the value obtained for $ZnAl_2O_4$ (see Table 2), independent of Zn loading or calcination temperature. Only weak sulfur peaks were seen in the ESCA spectra. This indicates the same lack of reactivity as was found for bulk $ZnAl_2O_4$.

For catalysts containing greater than 20% Zn, the reactivity was similar to bulk ZnO. After reaction with 15% H_2S/H_2 the Zn Auger parameter was within experimental error of the value obtained for ZnS. Intense S 2p and S 2s peaks with binding energies characteristic of ZnS also appeared in the ESCA spectra of these catalysts. For catalysts (>20% Zn) treated with 1.5% SO_2/air, the Zn Auger parameter and S 2p and S 2s binding energies indicated formation of $ZnSO_4$. XRD patterns of treated catalysts (either 15% H_2S/H_2 or 1.5% SO_2/air) showed no evidence of any sulfur compounds, regardless of Zn loading or calcination temperature.

The sulfiding studies are consistent with the spectroscopic studies, indicating an aluminate-like phase at low zinc loadings (<20%) and the presence of ZnO at higher loadings.

DISCUSSION

ESCA intensity ratio plots similar to Fig. 3 have been obtained previously for Ni/Al_2O_3 (*24*) and Co/Al_2O_3 (*25*) catalysts. Since the plot for zinc catalysts closely resembles those obtained for nickel and cobalt catalysts, it would appear that similar metal–support interactions occur in all

three systems. In the nickel and cobalt systems it was shown that at low metal loadings, the metal ions diffuse into the defect spinel lattice of γ-Al_2O_3, forming strong metal–support interaction species (*13, 24, 25*). For Ni/Al_2O_3 and Co/Al_2O_3 catalysts, these interaction species closely resemble bulk $NiAl_2O_4$ and $CoAl_2O_4$, and were referred to as "surface spinels." Formation of these "surface spinels" was favored by high calcination temperatures; the percentage of metal ions in the spinel form being greatest at low metal loadings. At high metal loadings, bulk-like metal–oxide phases (i.e., NiO, Co_3O_4) were found to segregate on the catalyst surface.

Results obtained for Zn/Al_2O_3 catalysts are consistent with the results for Ni/Al_2O_3 and Co/Al_2O_3. At low Zn loadings (<20%), ESCA binding energies indicated an interaction species which resembles bulk $ZnAl_2O_4$ (see Tables 2 and 3). The XRD and LRS results were consistent with the ESCA results, indicating formation of a spinel-like phase below 20% Zn. Bulk $ZnAl_2O_4$ reportedly forms more readily than either $CoAl_2O_4$ or $NiAl_2O_4$ (*13, 28*); hence, formation of a Zn "surface spinel" should occur more readily than for Ni or Co. Since formation of "surface spinels" has been observed on Ni/Al_2O_3 and Co/Al_2O_3 catalysts, results which indicate formation of a Zn "surface spinel" are not surprising. Although preparation of bulk aluminates usually requires long calcination times (several days) and high temperatures (>1000°C) (*2, 14*), the "surface spinels" apparently form under much milder conditions.

Due to the large tetrahedral (Td) site preference of Zn^{2+} ions (relative to ions such as Co^{2+}, Ni^{2+}, Cu^{2+}, Fe^{2+}, and Mn^{2+}), diffusion into the vacant Td sites of the γ-Al_2O_3 lattice occurs (*14*). Depending on calcination temperature and time, only a finite amount of zinc can be accommodated by the vacant Td lattice sites. Once all of the available lattice sites are saturated, further addition of zinc can be accommodated only by segregation of a separate ZnO phase. This phenomenon occurs at approximately 20% Zn, as the ESCA, XRD, and LRS results all indicated formation of a ZnO phase above 20% Zn.

Chin and Hercules have calculated that for Co/Al_2O_3 and Zn/Al_2O_3 catalysts, saturation of the surface (i.e., monolayer coverage) of their support (90 m^2/g) occurred at a metal content of approximately 10% (*3, 9, 25*). For the support used in this study (195 m^2/g), "monolayer" coverage should, therefore, occur at a zinc content of approximately 21%. The change in slope of the ESCA and ISS Zn/Al intensity ratio curves above 20% Zn (see Figs. 3 and 5) can be attributed to complete saturation of the lattice sites and indicates that a new zinc species (i.e., ZnO) occurs, at high Zn loading. The drastic increase in slope of the ESCA Zn/Al intensity ratio curve can be explained by a repartition of the ZnO phase on the external surface of the catalyst particle. The ZnO would then be more readily detected than the interaction species which would exist predominantly within the porosity of the support.

It was noted that at all concentrations both the ESCA and ISS Zn/Al intensity ratios were lower for catalysts calcined at 600°C than for those calcined at 400°C (see Figs. 3 and 5). This effect is related to the extent of metal–support interaction, i.e., as the calcination temperature is increased, a greater percentage of zinc ions can diffuse into the γ-Al_2O_3 lattice. If more zinc ions diffuse into the support, the Zn/Al intensity ratios should be lower, exactly as observed. Another possibility could be an increase in particle size due to increased sintering at the higher calcination temperature.

Comparing Figs. 3 (ESCA) and 5 (ISS), ISS shows a much larger difference in the Zn/Al intensity ratio between the two calcination temperatures than does ESCA. This can be attributed to the differences in the sampling depths between ESCA and ISS. The larger difference seen in the ISS plot indicates that, at constant Zn loading, the decrease in the amount of zinc on the sur-

face with increased calcination temperature is much greater over the sampling depth of ISS (ca. 3 Å), than it is over the sampling depth of ESCA (ca. 20 Å). This has important implications for catalysis since it is the uppermost layer of the catalyst surface that is involved in reactions. The results indicate that with increased calcination temperature, the uppermost surface layer is depleted of zinc to a greater extent than the outer 5–10 atomic layers due to increased diffusion of the zinc ions into the support. Hence, the catalytic activity would probably decrease at the higher calcination temperature to a greater extent than that expected from the ESCA data alone.

The fact that lowering of the ESCA and ISS intensity ratios was observed as the calcination temperature was increased, plus the fact that zinc was undetectable below 3% loading on catalysts calcined at 600°C, lend support to the subsurface nature of the interaction species and formation of a Zn "surface spinel."

The sulfidation experiments were consistent with the spectroscopic results. The high reactivity of bulk ZnO toward sulfur compounds is well known (*1, 6, 23*); however, results have shown that reactivity of $ZnAl_2O_4$ is low, reflecting the stability of Zn^{2+} ions in Td spinel sites. Similarly tetrahedrally coordinated Co^{2+} ions have been found to be unreactive toward H_2S sulfiding and H_2 reduction (*28*). This lack of reactivity may be attributed to the fact that both $ZnAl_2O_4$ and $CoAl_2O_4$ display considerable covalent character in the Zn–O and Co–O bonds, resulting in shorter than expected bond lengths (*6, 30*).

Reactivity of Zn/Al_2O_3 catalysts toward sulfiding was found to depend strongly on metal loading, indicating changes in surface composition. The low reactivity observed for catalysts with low zinc contents (<20%) can be attributed to formation of a Zn "surface spinel," resulting from diffusion of Zn^{2+} ions into vacant Td sites of the γ-Al_2O_3. The high reactivity observed for catalysts containing high zinc loadings (>20%) is consistent with the presence of a ZnO phase. Hence, the sulfiding results have important implications regarding the use of Zn/Al_2O_3 catalysts in desulfurization processes, indicating that catalysts with low zinc loadings (<20%) are poor sulfur sorbents compared to bulk ZnO and/or catalysts with high zinc loadings.

CONCLUSIONS

Several conclusions can be drawn from this study:

(1) The surface characteristics of Zn/Al_2O_3 catalysts are affected by both metal loading and calcination temperature.

(2) For Zn/Al_2O_3 catalysts having zinc contents below 20%, zinc ions interact strongly with the support forming a "surface spinel" which is similar in structure and reactivity to bulk $ZnAl_2O_4$.

(3) At high zinc content (>20%), segregation of another zinc species occurs. This zinc species is characterized as bulk-like ZnO.

(4) Zn/Al_2O_3 catalysts, as well as ZnO and $ZnAl_2O_4$ are unreactive to H_2 reduction at 500°C.

(5) ZnO and Zn/Al_2O_3 catalysts which contain a ZnO phase react with H_2S/H_2 and SO_2/air mixtures, forming ZnS and $ZnSO_4$, respectively. In contrast, $ZnAl_2O_4$ and catalysts consisting of only an "aluminate-type" phase show little or no reactivity to the above gas mixtures.

(6) The comparative ESCA, ISS, LRS, and XRD results demonstrate the complementary nature and value of these techniques for the study of supported catalysts.

ACKNOWLEDGMENTS

This work was partially supported by the National Science Foundation under Grant CHE-8108495. The authors wish to thank L. E. Makovsky of the Pittsburgh Energy Technology Center for obtaining the Raman spectra. We also thank Dr. M. Houalla for helpful discussions and suggestions.

REFERENCES

1. Thomas, C. L., "Catalytic Processes and Proven Catalysts." Academic Press, New York, 1970.

2. Vinek, H., Noller, H., Ebel, M., and Schwartz, K., *J. Chem. Soc. Faraday Trans. I* **73,** 734 (1977).
3. Chin, R. L., Ph.D. Dissertation, University of Pittsburgh, 1980.
4. Vinek, H., and Noller, H., *Z. Phys. Chem. (N.F.)* **102,** 247 (1976).
5. Vinek, H., and Noller, H., *Z. Phys. Chem. (N.F.)* **102,** 255 (1976).
6. Herman, R. G., Klier, K., Simmons, G. W., Finn, B. P., and Kobylinski, T. P., *J. Catal.* **56,** 407 (1979).
7. Pernicone, N., and Traina, F., *in* "Preparation of Catalysts II" (B. Delmon, P. Grange, P. Jacobs, and G. Poncelet, Eds.), p. 321–351. Elsevier, Amsterdam, 1978.
8. Cimino, A., Lo Jacono, M., and Schiavello, M., *J. Phys. Chem.* **79,** 243 (1975).
9. Chin, R. L., and Hercules, D. M., *J. Catal.* **74,** 121 (1982).
10. Strohmeier, B. R., Hercules, D. M., and Makovsky, L. E., to be published.
11. Weast, R. C. (Ed.), "Handbook of Chemistry and Physics," pp. B153–B154. CRC Press, Cleveland, 1973.
12. Patterson, T. A., Carver, J. C., Leyden, D. E., and Hercules, D. M., *J. Phys. Chem.* **80,** 1700 (1976).
13. Lo Jacono, M., and Schiavello, M., *in* "Preparation of Catalysts" (B. Delmon, P. A. Jacobs, and G. Poncelet, Eds.), pp. 474–487. Elsevier, Amsterdam, 1976.
14. Navrotsky, A., and Kleppa, O. J., *J. Inorg. Nucl. Chem.* **29,** 2701 (1967).
15. Cotton, F. A., and Wilkinson, G., "Advanced Inorganic Chemistry," 3rd Ed., p. 51. Wiley, New York, 1972.
16. Briggs, D. (Ed.), "Handbook of X-Ray and Ultraviolet Photoelectron Spectroscopy," pp. 390–391. Heyden, London, 1977.
17. Schön, G., *J. Electron Spectrosc.* **2,** 75 (1973).
18. Wagner, C. D., Gale, L. H., and Raymond, R. H., *Anal. Chem.* **51,** 466 (1979).
19. Shelef, M., Wheeler, M. A. Z., and Yao, H. C., *Surface Sci.* **47,** 697 (1975).
20. Zingg, D. S., Makovsky, L. E., Tischer, R. E., Brown, F. R., and Hercules, D. M., *J. Phys. Chem.* **84,** 2898 (1980).
21. Damen, T. C., Porto, S. P. S., and Tell, B., *Phys. Rev.* **142,** 570 (1966).
22. Jeziorowski, H., and Knözinger, H., *Chem. Phys. Lett.* **51,** 519 (1977).
23. Westmoreland, P. R., and Harrison, D. P., *Environ. Sci. Technol.* **10,** 659 (1976).
24. Wu, M., and Hercules, D. M., *J. Phys. Chem.* **83,** 2003 (1979).
25. Chin, R. L., and Hercules, D. M., *J. Phys. Chem.* **86,** 360 (1982).
26. Strohmeier, B. R., and Hercules, D. M., unpublished results, University of Pittsburgh, 1982.
27. Vogel, R. F., Mitchell, B. R., and Massoth, F. E., *Environ. Sci. Technol.* **8,** 432 (1974).
28. Chin, R. L., and Hercules, D. M., *J. Phys. Chem.* **86,** 3079 (1982).
29. Navrotsky, A., and Kleppa, O. J., *J. Inorg. Nucl. Chem.* **30,** 479 (1968).
30. Porta, P., and Anichini, A., *Z. Phys. Chem. Neue Folge* **127,** 223 (1981).